Journal of Mines, Metals and Fuels, *73(4): 1121-1134; 2025. DOI: 10.18311/jmmf/2025/48385*

Print ISSN : 0022-2755

Journal of Mines, Metals and Fuels

Contents available at: *www.informaticsjournals.co.in/index.php/jmmf*

Effects of Various Fuels on the Qualified Photoluminescence and Thermoluminescence Properties of $BaZrO_3$ Nanophosphors

T. N. Silpa[1], C. Pandurangappa[1], Yashaswini[2], S. Pratibha[3]* and A. Jayasheelan[4]

[1]Department of Physics, R. N. S. Institute of Technology, Bangalore - 560098, Karnataka, India
[2]Department of Physics, BMS Institute of Technology and Management, Bangalore - 560064, Karnataka, India
[3]Department of Physics, BMS College of Engineering, Bangalore - 560019, Karnataka, India; s.pratibha.87@gmail.com
[4]Department of Physics, Maharani Science College for Women, Bangalore - 560001, Karnataka, India

Abstract

Glycine, urea, and citric acid are used as fuels in the simple combustion process to create Barium Zirconate ($BaZrO_3$) (BAZ) nanophosphors, which are the subject of the qualified photoluminescence and thermoluminescence studies reported in this work. Using fundamental methods, the size, structure, and purity of the nanophosphors were assessed. Powder X-ray Diffraction (PXRD) spectra verified the cubic structure with space group Pm-3m and JCPDS card number 06-0399. Vibrational stretching of Zr-O bonds is explained by the strong peaks at 492-686 cm^{-1}, while Fourier Transform Infrared microscopy (FTIR) spectra showed vibrational modes of Ba-O, which are metal oxide bonds, at 1465-1168 cm^{-1}. SEM, or Scanning Electron Microscopy, shows that the processed materials have formed nanoparticles. The UV Intrinsic defects, crystal structure, energy transfer processes, and temperature effects all work together to influence the blue emission in $BaZrO_3$ by generating localised energy states, promoting transitions, and influencing the efficiency of radiative recombination. The Photoluminescence (PL) emission spectra of BAZ nano powders up on 370 nm excitation revealed bluish emissions at 425 nm. The production of bluish phosphors is validated by the chromaticity coordinates. Thermoluminescence (TL) properties of BAZ nano particles subjected to 500Gy and 2KGy dosages were investigated. The kinetic parameters were determined, and the second order kinetics were validated by the produced powders TL glow curve.

Major Findings: *BAZ nanophosphors were successfully fabricated utilizing three distinct fuels. The luminescence features of the synthesized phosphors were discussed in detail. The prepared phosphors are good candidates for solid-state lightning and dosimteric applications.*

Keywords: Combustion; Nanoparticles, Nanophosphors, Photoluminescence, Thermoluminescence

1.0 Introduction

The luminescent features of perovskites like $BaZrO_3$ have drawn the attention of researchers, scientists, and technologists in recent years due to their numerous applications. On BAZ, a few spectroscopic investigations have been conducted[1-4]. To the best of our knowledge, no research studying the production and luminescence of BAZ nanophosphors using three distinct fuels by burning technique has been published. In order to investigate the structure and luminescence of BAZ nanophosphors using three distinct fuels through combustion, the current work has been undertaken. Understanding perovskite materials is exceptionally vigorous field of study that

**Author for correspondence*

has attracted continual attention over the years and is crucial for both practical applications and basic related problems[5-7].

The general formula ABX_3 represents the perovskite family, where X is an anion and A and B are cations. Reports state that the smaller tetravalent B cation is located in the heart of the corner-sharing BO_6 octahedron in the perovskite oxide structure, whereas the larger divalent A cation is located in the cavities between eight octahedrons with a 12-fold oxygen coordination. Numerous intriguing electrical, mechanical, and conductive characteristics are displayed by the perovskite oxide material. BAZ possesses outstanding electrical, optical, mechanical, and thermal properties, a broad energy gap, a high refractive index, and strong photochemical stability[8-11]. The tetravalent cation in $BaZrO_3$ matches the B-site very exactly. It should be mentioned that these materials have cubic symmetry and a Goldschmidt tolerance factor of roughly one[12]. Bilic and Gale used density-functional theory calculations to study the ground state characteristics of BAZ[13]. BAZ was studied both theoretically and experimentally by Akbarzadeh *et al*. at low temperatures[14]. The radio luminescence characteristics of deca-octahedral BAZ nanocrystals were investigated by Moreira *et al*[15]. BAZ has been the subject of numerous studies to gather structural data using a variety of spectroscopic techniques[16-22]. One of the major factors to prepare nanophosphors with enhanced luminescence properties in combustion technique is the type of fuel. To synthesize perovskites like BAZ, the common fuels choice are glycine, urea and citric acid. To the best of our knowledge, limited number of research articles on the synthesis and optical characteristics of BAZ nanophosphors using the combustion approach with three distinct fuels.

As a result, a thorough analysis of the produced BAZ nanophosphors utilising three distinct fuels and the combustion process is conducted, utilising characterisation methods such as XRD, SEM, FTIR, UV, and optical characteristics by photoluminescence and thermoluminescence studies.

2.0 Materials and Methods

$BaZrO_3$ was prepared with three different fuels by the combustion synthesis method.

2.1 Sample Preparation

The combustion synthesis method was used to create the BAZ nanoparticles using three distinct fuels. The precursors were stoichiometric amounts of $BaNO_3$, ZrO (NO_3), and the fuels were glycine, urea, and citric acid. The total oxidising and reducing valences of the Fuel (F) and the Oxidiser (O) have been used to compute the stoichiometric composition of the redox mixes. Initially, 30 millilitres of deionised water were used to dissolve the reactants in their stoichiometric ratio while stirring constantly. The aforementioned solution was then mixed with a determined amount of fuel, specifically glycine, while keeping the oxidiser to fuel ratio at 1. To create a uniform transparent solution, the resulting mixture was vigorously stirred with a magnetic stirrer. The mixtures were then kept to 450°C for 15 minutes in a muffle furnace that had been preheated. It is anticipated that the combustion synthesis process will be finished in a few minutes. An agate mortar and pestle were used to smash the resulting BAZ coarsely. After that, the product was calcined for two hours at 900°C. The creation of BAZ nanoparticles using the remaining fuels, urea and citric acid, follows the same process.

2.2 Characterization

PXRD measurements of the produced materials were used to analyse the structure using the Rigaku Smart Lab, which has a Ni filter and Cu-Kα radiation. A Perkin-Elmer (FTIR) spectrometer was used to generate nanophosphors spectra, which were in the 4000-400 cm^{-1} range. Using SEM-JEOL JSM-840A the surface morphology of these nanophosphors was evaluated. Elemental sharing confirmed by energy dispersive spectroscopy analysis. A UV-1800 UV-V is spectrophotometer was used to record the absorption spectra in the UV-visible band. An Agilent Cary-eclipse spectrofluorometer was used to perform the PL spectroscopic analyses. The Nucleonix TL reader device was used to note the produced nanophosphors TL response.

3.0 Results and Discussion

3.1 Powder X-Ray Diffraction (PXRD)

A simple cubic crystallographic structure with the space

group Pm-3m is existing in the diffraction pattern for BAZ nanophosphors shown in Figure 1, with lattice parameters of a = b = c = 4.1930 Å. Strong agreement is seen between the diffraction peak alignment and the standard data for BAZ (JCPDS Card no. 00-006-0399). The strong, powerful peaks that were clearly visible indicate that the processed samples had a high degree of crystallinity. The primary peaks correspond to the following principal lattice planes (hkl): (100), (110) (111), (200), (211), (220), (310) and (022). The Miller indices consistency with the body of current research must be emphasised[23]. There were no impurity-related peaks found.

The average crystallite size was determined by utilizing Scherer's equation which is given as[24]

$$D = \frac{K\lambda}{\beta\cos\theta} \quad (1),$$

where θ is the Bragg's angle or diffraction angle, β is the diffracted full width half maximum intensity (FWHM) in radians, λ is the incident wavelength of the Cu-Kα (0.154 nm) line, and D is the average grain size of the crystallites. This method yielded an average crystallite size between 34 and 45 nm, confirming the generated materials nano regime. The Equation (2) was used to calculate the average size of crystallites using the line broadening technique in PXRD using the W-H method[25].

$$\beta\cos\theta = \varepsilon(4\sin\theta) + \lambda/D \quad (2),$$

where D is the grain size, ε is the developed strain, and β (FWHM) in radians is the measurement of distinct XRD peaks that correspond to distinctplanes. Figure 2 displays the W-H plots for BAZ nanophosphors. The typical

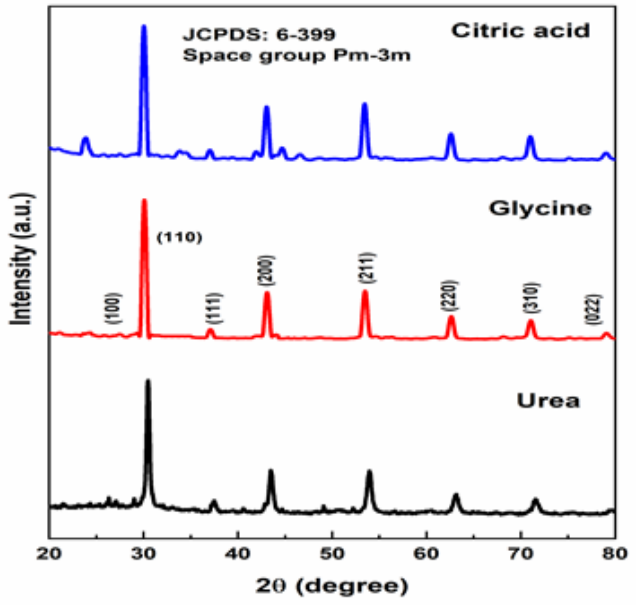


Figure 1. PXRD pattern of $BaZrO_3$ nanophosphors.

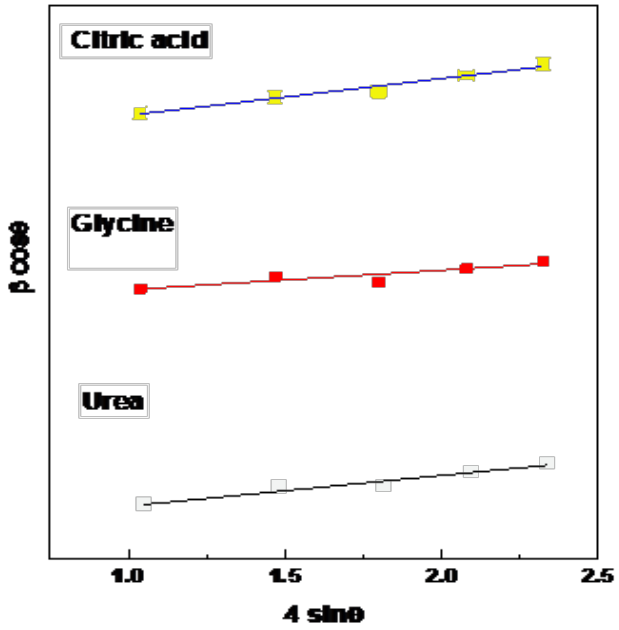


Figure 2. W-H graph of $BaZrO_3$ nanophosphors.

Table 1. Estimated values of average crystallite size, and band gap of $BaZrO_3$ nanophosphors

Sample	Crystallite Size		Energy Band Gap (eV)
	Scherer Method	W-H Method	
BAZ (C)	34	36	2.31
BAZ(G)	32	34	3.17
BAZ(U)	45	49	2.45

crystallite size is between 34 and 49 nm. The incremental rise in crystallite dimensions when compared to the Scherrer's technique is ascribed to the incorporation of a strain component and it is not considered in the Scherrer's equation. The dimensions of the crystallite and the lattice strain of the synthesized nanophosphors are outlined in Table 1.

3.2 Fourier Transforms Infrared Spectroscopy (FTIR)

FTIR spectra were examined to assess the material's absorption bond and functional groups. The FTIR spectra of BAZ nanopowders in the 4000-500 cm^{-1} region is displayed in Figure 3. The acquired FTIR spectrum shows that the 1500-4000 cm^{-1} region is especially analysed for the functional groups contained in the material. The vibrational stretching related to Zr-O bonds, is explained by the number of peaks found in the 492-686 cm^{-1} range[26]. The collection of peaks found in the 1465-1168 cm^{-1} range is ascribed to the sample's Ba-O bond vibrational modes.

The extremely low intensity peaks, which are centred between 3204 cm^{-1} and 3890 cm^{-1}, demonstrate that the synthesised perovskites contain a very little amount of moisture. The sample's H-O starching from potential absorption of ambient moisture is the cause of a little peak at a higher wavenumber. Regardless of the synthesis method, residual water and hydroxy groups are typically found in the prepared samples, and their removal

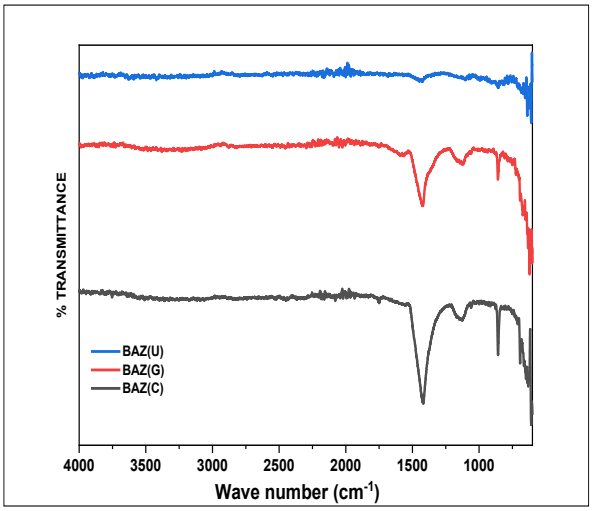
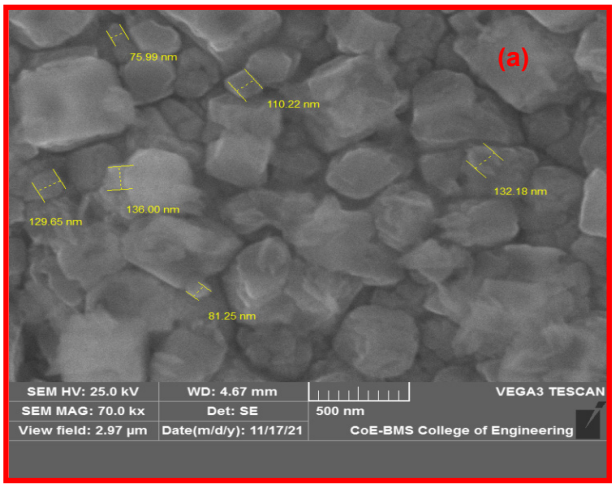
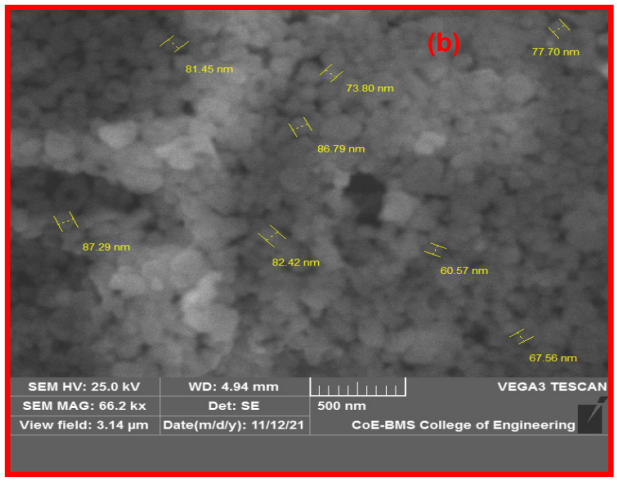


Figure 3. FTIR spectra of $BaZrO_3$nanophosphors.





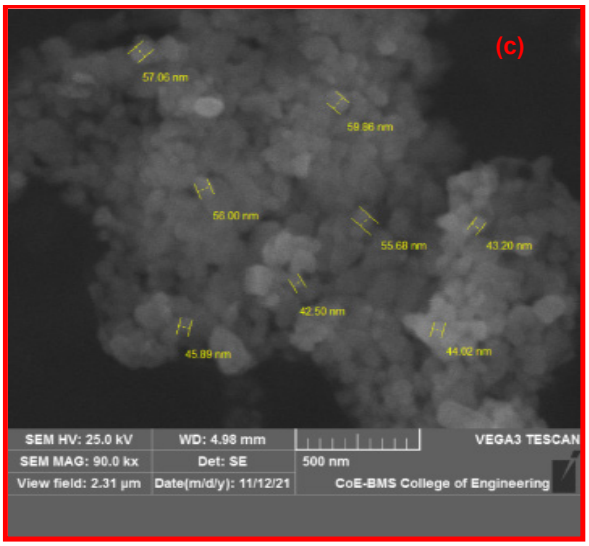


Figure 4. SEM images of **(a)** $BaZrO_3$(U) **(b)** $BaZrO_3$ (G) **(c)** $BaZrO_3$(C) nanophosphors.

requires additional heat treatment. The synthesis and purity of BAZ phosphor are confirmed by the combined observation of all these peaks.

3.3 Morphological Studies

Understanding the morphology of the synthesised material requires the use of scanning electron microscopy. Figure 4 displayed the shape of BAZ nanophosphors. Additionally, the SEM pictures show that there are nanoparticles of both smaller and larger sizes, with diameters ranging from 42 nm to 132 nm. Thus, these nanoparticles have an average diameter of about 80 nm and a length of a few tens of μm. The BAZ nanophosphor's EDS elemental mapping is shown in Figure 5. The elements mapping shows that Ba, Zr, and O were evenly distributed.

Glycine's combustion properties as a combustion agent can be attributed to the smaller particle size that was attained during the manufacture of BAZ nanophosphor as compared to urea and citric acid. Glycine is known for its capacity to promote a faster and more intense combustion process, which raises the temperature and speeds up the synthesis process. Greater gas production from the glycine-induced combustion event may result in increased porosity and light diffusion in the nanophosphor, which would affect the final particle size[27].

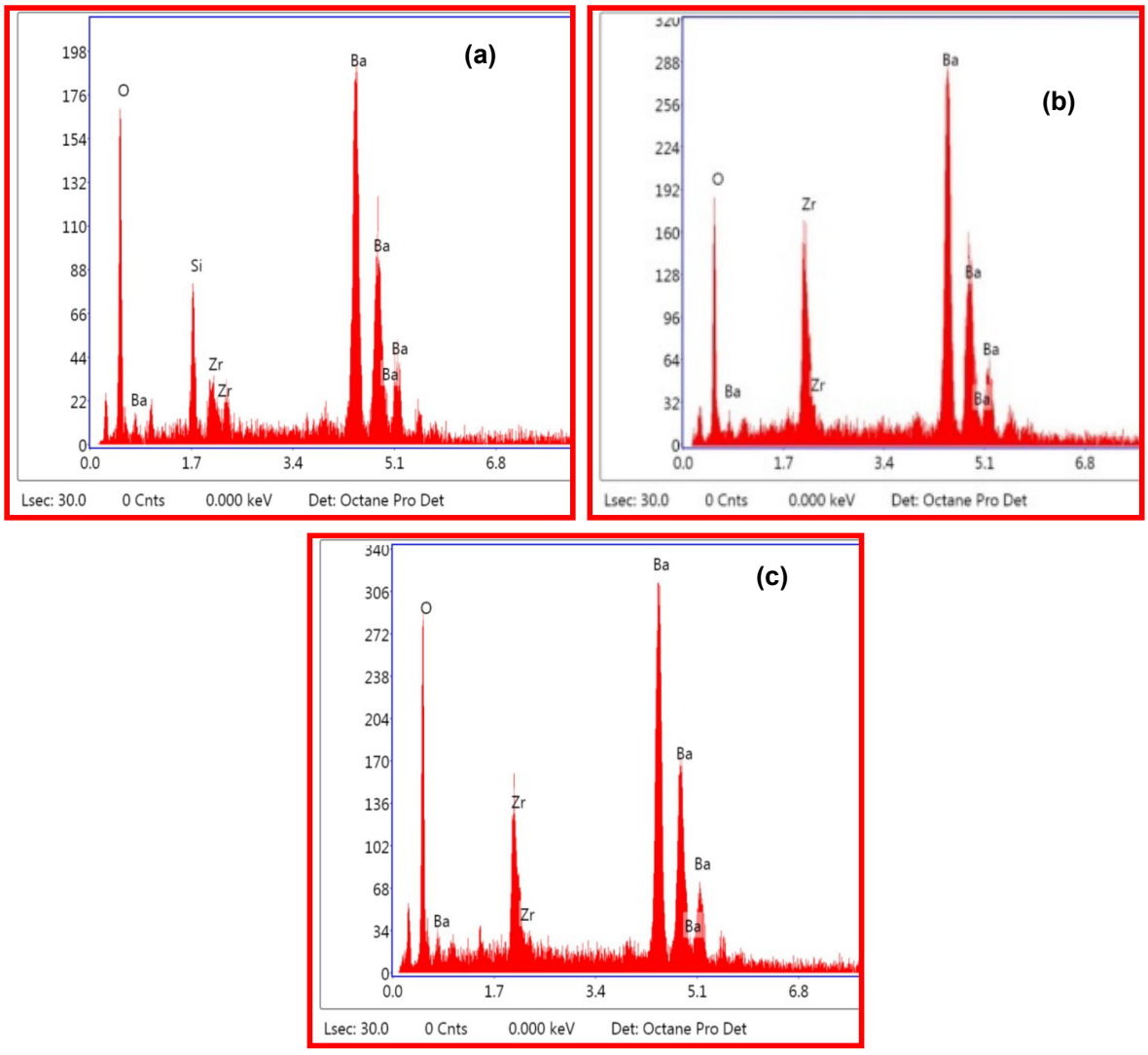


Figure 5. EDS spectra of **(a)** $BaZrO_3$(U) **(b)** $BaZrO_3$(G) **(c)** $BaZrO_3$(C) nanophosphors.

3.4 Diffuse Reflectance Spectroscopy

The optical band gap of the prepared nanophosphors is as indicated in Figure 6, and values are estimated for different fuels based BAZ nanophosphors utilizing DRS spectroscopy by means of Kubelka-Munk (K-M) model.

$$F(R_\infty) = \frac{(1-R_\infty)^2}{2R_\infty} \quad (3)$$

where, F(R) : K-M function which is relative to absorption coefficient and R: reflectance.

$$\text{Or} \quad h\nu = \frac{1240}{\lambda} \quad (4)$$

The estimated optical band gap of the synthesized nanophosphors was found to be 2.31 – 3.17 eV.

3.5 Photoluminescence

3.5.1 Photoluminescence of Undoped BAZ

Figure 7 and Figure 8 display the excitation and emission spectra of BAZ nanophosphor. The excitation spectrum was noted by maintaining the emission wavelength at

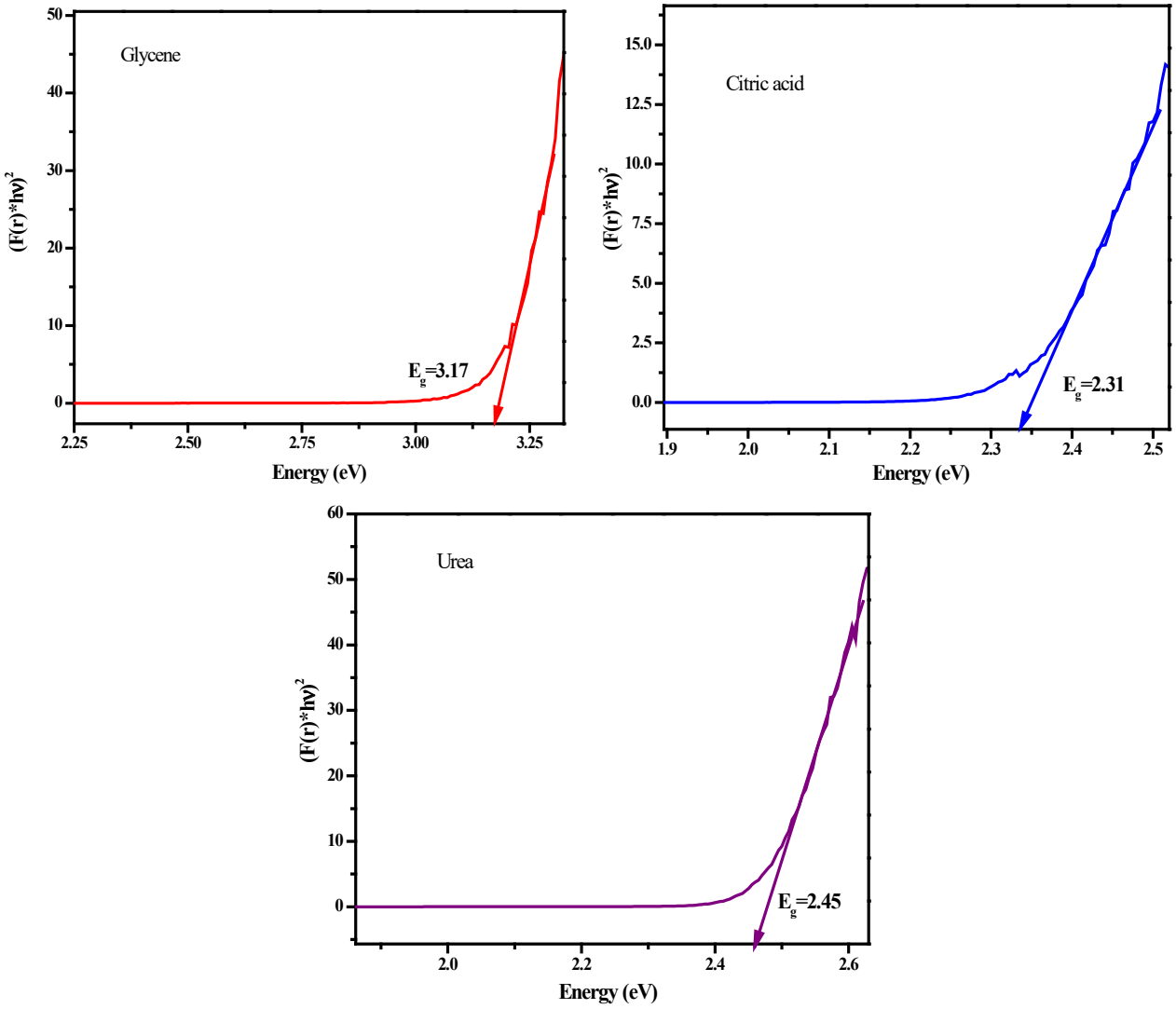


Figure 6. DRS spectra of **(a)** $BaZrO_3$(U) **(b)** $BaZrO_3$(G) **(c)** $BaZrO_3$(C) nanophosphors.

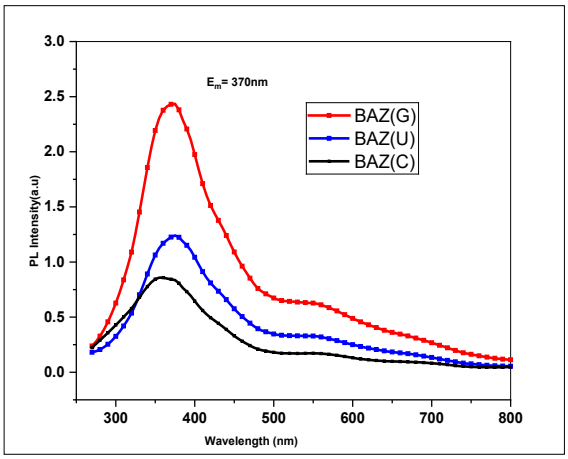


Figure 7. Excitation spectra of **(a)** $BaZrO_3$(U) **(b)** $BaZrO_3$(G) **(c)** $BaZrO_3$(C) nanophosphors.

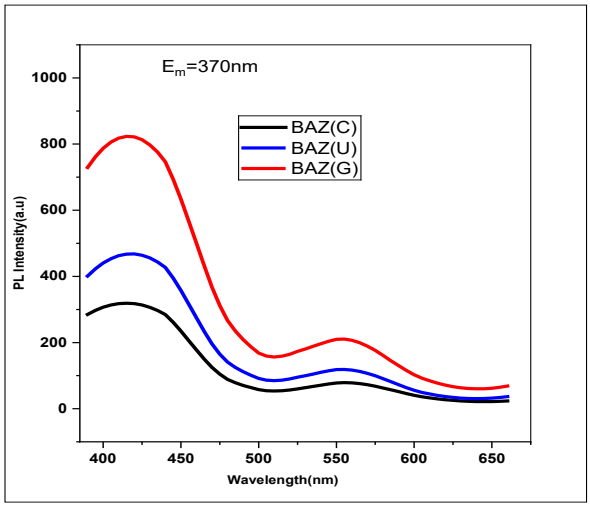


Figure 8. Emission spectra of **(a)** $BaZrO_3$ (U) **(b)** $BaZrO_3$ (G) **(c)** $BaZrO_3$ (C) nanophosphors.

425 nm, which is associated with the change from energy levels 5d to 4f. There are noticeable peaks in this excitation spectra at 370 nm[28].

When exposed to a UV excitation wavelength of 370 nm, the photoluminescence emission spectra of BAZ nanophosphors revealed a strong emission peak at 425 nm, which falls inside the visible spectrum's blue area and is commonly used as a blue-emitting phosphor in lighting and display applications. In undoped BAZ nanoparticles, charge carrier recombination involving electron transitions from the conduction to valence band is responsible for the blue emissions at 425 nm.

This process is accelerated by localised energy states produced by crystal lattice defects, which helps explain the observed blue emission[29]. The development of the oxygen shortage is also confirmed by the appearance of a broad and powerful blue emission that is centred at 550 nm[30].

Several aspects of the combustion synthesis process can be blamed for the increased Photoluminescence (PL) intensity shown in BAZ produced with glycine as a fuel as opposed to urea and citric acid. As a fuel, glycine encourages a more effective combustion reaction, which raises the maximum temperature, improves crystallisation, and reduces the size of the resulting crystallites. Urea and citric acid, on the other hand, cause longer ignition periods and lower combustion temperatures, which may have an adverse effect on the homogeneity and crystallinity of the produced particles[31]. Furthermore, it has been demonstrated that citric acid inhibits the production of combustion, which may result in the development of less desirable structural features in the finished product[32]. The PL qualities of the produced materials may also be diminished by the presence of carbon impurities and organic fragments from citric acid[33].

Consequently, compared to the other fuels utilised, the superior PL intensity in BAZ synthesised with glycine is probably caused by its capacity to provide ideal combustion conditions, which leads to better crystallisation and fewer impurities[32,33]. The band gap as estimated by using the PL data is found to be 3.35 eV which is in agreement with the DRS spectroscopy data.

3.5.2 Chromaticity Coordinates

The colour of the phosphor's emission can be determined using the Commission Internationale de l'Eclairage (CIE) chromaticity using the chromaticity coordinates (x, y)[34,35]. Table 2 displays the calculated CIE values for BAZ nanophosphors at an excitation wavelength of 370 nm. As seen in Figure 9 the CIE diagram for BAZ nanophosphors with acquired CIE colour coordinates under 370 nm excitation displays a blue hue. The findings show that the compounds with dominant PL intensity and blue luminescence meet the NTSC standard values (x = 0.22, y = 0.177). Additionally, the blue emission in

Table 2. Estimated CIE values for BAZ nanophosphors at an excitation wavelength of 370 nm

Sample	X	Y	U	v	n	CCT (K)
BAZ(C)	0.223	0.177	0.191	0.34	0.70513	2313.65
BAZ(G)	0.22	0.178	0.187	0.341	0.72903	2256.98
BAZ(U)	0.219	0.177	0.187	0.34	0.73077	2252.98

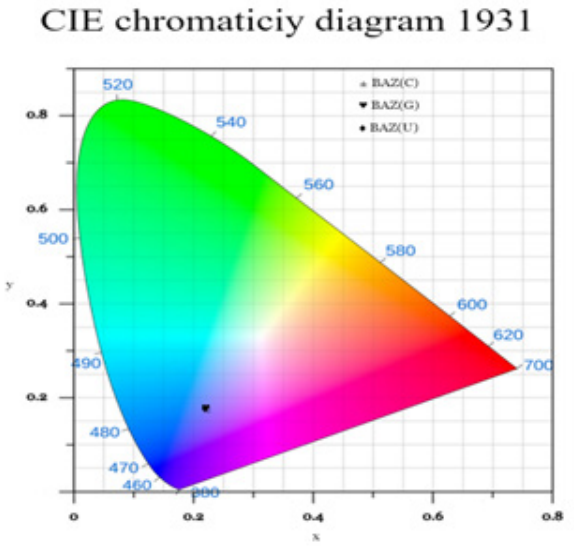


Figure 9. CIE diagram of undoped $BaZrO_3$ nanophosphors.

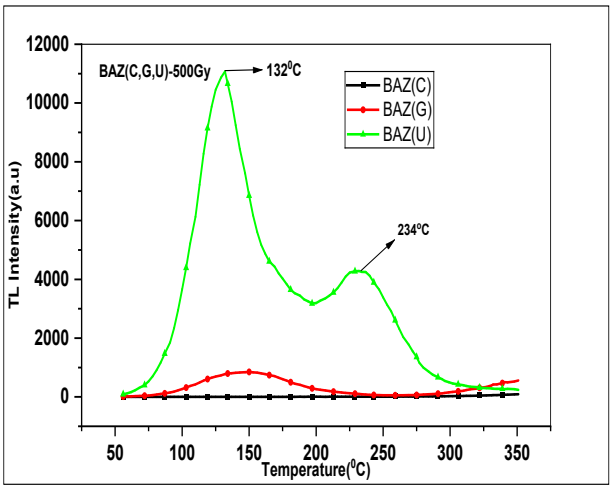


Figure 10. TL glow curve of undoped $BaZrO_3$ nanophosphors irradiated by 500 Gy.

the visible spectra was validated by a colour chromaticity investigation. The phosphors, which are used in the production of near UV-LED's and display devices, demonstrated an average CCT of 2274 K, making them "soft white" compact fluorescent and LED lamps. As a result, the produced nanophosphors might find use in display devices.

3.6 Thermoluminescence

3.6.1 TL Glow Curves

TL glow curves of BAZ (U, G, and C) nanophosphor subjected to 500 Gy and 2k Gy γ-dose (^{60}Co) are shown in Figure 10 and Figure 11. The temperature-dependent TL glow curve is used to evaluate light intensity. The TL technique's glow curves are crucial for determining whether a material is suitable for radiation dosimetry[36-49].

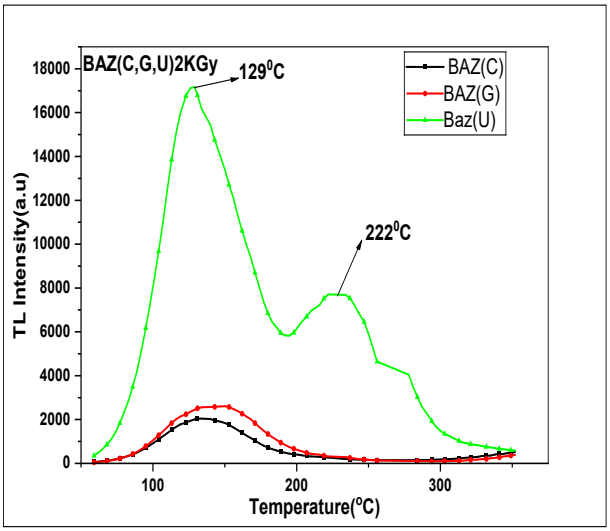


Figure 11. TL glow curve of undoped $BaZrO_3$ nanophosphors irradiated by 2k Gy.

The TL properties of BAZ nanophosphors exposed to γ-irradiation were examined.

At a warming rate of 30Cs^{-1}, two peaks in the TL glow curve of $BaZrO_3$ (U) were detected: one at 132° C (Intense) and one at 234° C (Shouldered). The image makes it clear that the glow peak temperature at 132° C was more important than the glow peak at 234° C peak, suggesting that more charge carriers were trapped at narrow defect levels. This could be because trapping is associated with deeper defect levels.

3.6.2 TL Kinetic Parameters

The BAZ (U) nano phosphor exhibited the highest TL intensity when exposed to radiation, as demonstrated by the 2 mg irradiated sample that was obtained each time for the TL spectra measurement. Kinetic parameters like E, b, s, no, and τ are the primary determinants of the phosphors dosimetric characteristics. Estimating the kinetics parameters is crucial for dosimetric applications to determine the deep level of flaws and TL characteristics. The stability of luminous centres is demonstrated by these values (E, b, s, no, and τ).

Thus, using various techniques, the kinetic parameters were estimated for the glow peak dosed at 500 Gy and 2k Gy. As shown in Figure 12 and Figure 13, the glow curves of BAZ (U) were de-convoluted using Origin pro8 software prior to the determination of kinetic parameters. Additionally, the de-convolution of the glow peak for BAZ (G,C) exposed to 500 Gy and 2k Gy doses follows the same method. The kinetic parameters of each deconvoluted glow curve of the TL materials, including the order of kinetics (b), activation energy (E), frequency factor (s), concentration of trapped charges (no), and life time of the traps (τ), were determined using the peak shape method, also referred to as Chen's method[50]. The values of E, b, s, no, and τ demonstrated the stability of luminous centres. Lushchik's and Halperin and Braner's peak shape approaches were also employed in the present work[51,52].

The temperature Tm, T_1, and T_2 are the main determinants of this peak shape approach. Tm is the temperature at the highest TL intensity, while T_1 and T_2 are the temperatures that correspond to half of the intensities on either side of the glow peak's maximum, respectively. The equation is used to theoretically estimate the order of kinetics (b) depending on the value of the symmetric factor (μg).

$$\mu_g = \frac{T_2 - T_m}{T_2 - T_1} \quad (5)$$

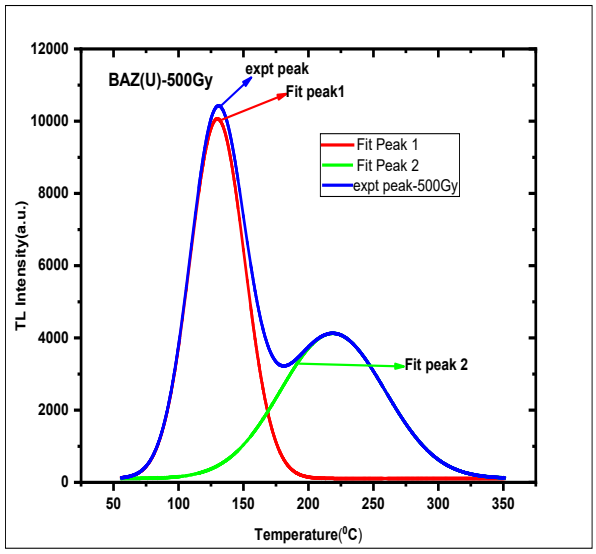


Figure 12. Deconvoluted glow curve of BAZ(U).

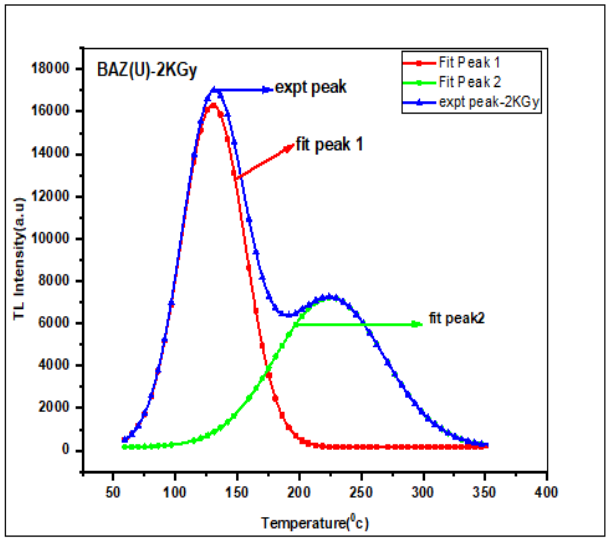


Figure 13. Deconvoluted glow curve of 2K Gy irradiated BAZ(U).

The value is around 0.42 for I order kinetics and 0.52 for II order kinetics[53]. Three techniques have been employed in this work to determine the activation energy. They are Chen's formula, the Halperin and Braner method, and the Luschik approach[54]. The following formula can be used to determine the activation energy in the Luschik method:

$$E = \frac{2kT_m^2}{\delta} \quad (6)$$

where $\delta = T_2 - T_m$.

In Halperin and Braner method, the activation energy can be[55]

$$E = \frac{2kT_m^2(1-3\Delta)}{\delta} \quad (7)$$

where, $\Delta = 2kT_m/E$ and $\tau = T_m - T_1$.

The activation energy can be calculated by Chen's formula[56]

$$E = \frac{2kTm(1.76Tm)}{\omega - 1} \quad (8)$$

where $\omega = T_2 - T_1$.

Randall and Wilikins derived an equation for the estimation of the frequency factor for all these methods and is given by[57]

$$\frac{\beta E}{kT_m^2} = s\, e^{-\frac{E}{kT}} \quad (9)$$

where β is the linear heating rate.

Further, the concentration of trapped charges (no) is determined by using the equation[58]

$$no = \frac{\omega I_m}{\beta(2.52 + 10.2(\mu g - 0.42))} \quad (10)$$

where I_m is the glow peak intensity.

The lifetime of the traps can be estimated using the relation[59]

$$\tau = S^{-1} e^{\frac{E}{kT}} \quad (11)$$

When exposed to gamma radiation, the Thermoluminescence (TL) response of BAZ which is produced using the fuels glycine, urea, and citric acid-displays significant variability. The computed kinetic parameters are listed in Table 3 and Table 4. The most noticeable TL response is shown by the BAZ derived from urea, which is followed by glycine and citric acid. BAZ nanoparticles were synthesized with urea yielding the good structural characteristics, thereby enhancing the TL response through enhanced crystallinity and defect concentration. The cubic crystalline architecture was confirmed through X-ray diffraction analysis, suggesting that the selection of fuel significantly impacts the micro structural attributes of the material. Under gamma radiation exposure of 500 Gy and 2k Gy the TL response was markedly elevated for samples derived from urea,

Table 3. Estimated kinetic parameters of $BaZrO_3$ nanophosphors irradiated by 500 Gy

Sample	Peak	T_m	μ_g	Order of Kinetics	Activation Energy(eV)				Frequency Factor (s) in Hz	Concentration of Trapped Charges(n_o) (m^{-3})	Life Time (τ) ms
					E_τ	E_δ	E_ω	E			
BAZ(C)	A	150	0.48	2	0.35	0.53	0.46	0.45	259951.294	3488.75748	9574.05
BAZ(G)	A	155	0.50	2	0.39	0.55	0.49	0.48	309381.739	1297.69308	9574.05
BAZ(U)	A	152	0.49	2	0.39	0.56	0.5	0.49	545365.712	1784.8171	9183.27
	B	150	0.48	2	0.42	0.59	0.53	0.51	1543306.48	1954.90277	8597.11

Table 4. Estimated kinetic parameters of $BaZrO_3$ nanophosphors irradiated by 2k Gy.

Sample	peak	T_m	μ_g	Order of Kinetics	Activation Energy(eV)				Frequency Factor (s) in Hz	Concentration of Trapped Charges(n_o) (m^{-3})	Life Time (τ) ms
					E_τ	E_δ	E_ω	E			
BAZ(C)	A	137	0.47	2	0.60	0.77	0.69	0.69	497523244	15005.5905	6252.44
BAZ(G)	A	143	0.5	2	0.55	0.68	0.63	0.62	29586206	20052.7578	7229.38
BAZ(U)	A	130	0.49	2	0.69	0.82	0.766	0.76	3489363398	98734.003	5666.27
	B	228	0.47	2	0.53	0.76	0.66	0.65	5768587.03	80442.029	9378.66

which can be attributed to the improved trap levels and energy distribution characteristics[60].

On the other hand, samples made from citric acid and glycine showed reduced TL responses, which might be because of differences in trap depth and less effective energy transfer pathways[60-62].

4.0 Conclusion

The low temperature solution combustion approach was successfully used to create the BAZ nanophosphors. Nanophosphors luminous characteristics and structural analysis were thoroughly examined. Using Powder X-ray Diffraction (PXRD) spectra, the cubic structure with space group Pm-3m and JCPDS card number 06-0399 was verified. Fourier Transform Infrared Microscopy (FTIR) spectra showed that the strong peaks at 492-686 cm^{-1} represent the vibrational stretching of Zr-O bonds, while the vibrational modes of Ba-O, which are metal oxide bonds, were found at 1465-1168 cm^{-1}. Nanoparticle production for the prepared materials is revealed by Scanning Electron Microscopy (SEM). The photoluminescence spectra demonstrated how well NUV light could stimulate these nanophosphors. The transition from energy levels 5d to 4f is responsible for the emission wavelength at 425 nm. Additionally, the blue emission in the visible spectra was validated by a colour chromaticity investigation. Under 370 nm excitation, the phosphors demonstrated an average CCT of 2274 K, making them "soft white" compact fluorescent and LED lamps that are widely used in the production of near UV-LED's and display devices. In contrast to BAZ (U), which has a significant glow peak clearly defined at 131° C upon γ-irradiation of 500 Gyat and 129° C upon γ-irradiation of 2k Gy, the BAZ (C) nanophosphors exhibit a weak TL response, according to TL research. BAZ (U, G, and C) nanophosphor TL glow curves for 500 and 2k γ-doses were examined, and their kinetic parameters were computed. From the experimental studies it is observed that, BAZ (G) exhibits higher PL intensity whereas BAZ (U) nanophosphor was shown to respond well to both 500 Gy and 2k Gy γ-irradiation. These findings imply that the produced nanophosphors may find value in dosimetric, lighting, and display applications.

5.0 References

1. Mari B, Singh KC, Sahal M, Khatkar SP, Taxak VB, Kumar M. Preparation and luminescence properties of Tb^{3+} doped ZrO_2 and $BaZrO_3$ phosphors. J Lumin. 2010; 130(11):2128-2132. https://doi.org/10.1016/j.jlumin.2010.06.005
2. Guo L, Zhong C, Wang X, Li L. Synthesis and photoluminescence properties of Er^{3+} doped $BaZrO_3$ nanotube arrays. J Alloys Compd. 2012; 530:22-25. https://doi.org/10.1016/j.jallcom.2012.03.092
3. Liu X, Wang X. Preparation and luminescence properties of $BaZrO_3$: Eu phosphor powders. Opt Mater. 2007; 30(4):626-629. https://doi.org/10.1016/j.optmat.2007.02.032

4. Hinatsu Y, Edelstein N. Electron paramagnetic resonance spectra of Pr^{4+} ions doped in $BaMO_3$ (M=Ce, Zr, Sn) and $SrCeO_3$. J Alloys Compd. 1997; 250(1-2):400-404. https://doi.org/10.1016/s0925-8388(96)02557-1
5. Iwahara H, Asakura Y, Katahira K, Tanaka M. Prospect of hydrogen technology using proton-conducting ceramics. Solid State Ion. 2004; 168(3-4):299-310. https://doi.org/10.1016/j.ssi.2003.03.001
6. Woodward PM. Octahedral tilting in perovskites. II. Structure stabilizing forces. Acta Cryst B. 1997; 53(1):44-66. https://doi.org/10.1107/s0108768196012050
7. Ravi V, Kutty TRN. Influence of cubic perovskite phase content on the positive temperature coefficient of resistance of n-type $BaTiO_3$ ceramics. Mater Sci Eng B. 1991; 10(1):41-52. https://doi.org/10.1016/0921-5107(91)90093-b
8. Bennett JW, Grinberg I, Rappe AM. Effect of substituting of S for O: The sulfide perovskite $BaZrS_3$ investigated with density functional theory. Phys Rev B. 2009; 79(23):235115. https://doi.org/10.1103/physrevb.79.235115
9. Boschini F, Rulmont A, Cloots R, Vertruyen B. Rapid synthesis of submicron crystalline barium zirconate $BaZrO_3$ by precipitation in aqueous basic solution below 100° C. J Eur Ceram Soc. 2009; 29(8):1457-1462. https://doi.org/10.1016/j.jeurceramsoc.2008.09.001
10. Chen X, Rieth L, Miller MS, Solzbacher F. High temperature humidity sensors based on sputtered Y-doped $BaZrO_3$ thin films. Sens Actuators B: Chem. 2009; 137(2):578-585. https://doi.org/10.1016/j.snb.2009.01.024
11. Duval SBC, Holtappels P, Vogt UF, Stimming U, Graule T. Characterisation of $BaZr_{0.9}Y_{0.1}O_{3-\delta}$ prepared by three different synthesis methods: Study of the sinterability and the conductivity. FC. 2009; 9(5):613-621. https://doi.org/10.1002/fuce.200800170
12. Goudochnikov P, Bell AJ. Correlations between transition temperature, tolerance factor and cohesive energy in 2+:4+ perovskites. J Physics: Condens Matter. 2007; 19(17):176201. https://doi.org/10.1088/0953-8984/19/17/176201
13. Bilic A, Gale JD. Ground state structure of BaZrO3: A comparative first-principles study. Phys Rev B. 2009; 79(17):174107. https://doi.org/10.1103/physrevb.79.174107
14. Akbarzadeh AR, Kornev I, Malibert C, Bellaiche L, Kiat JM. Combined theoretical and experimental study of the low-temperature properties of $BaZrO_3$. Phys Rev B. 2005; 72(20):205104. https://doi.org/10.1103/physrevb.72.205104
15. Moreira ML, Volanti DP, Andres J, Montes PJR, Valerio MEG, Varela JA, Longo E. Radioluminescence properties of decaoctahedral $BaZrO_3$. Scr Mater. 2011; 64(2):118-121. https://doi.org/10.1016/j.scriptamat.2010.09.017
16. Chen X, Rieth L, Miller MS, Solzbacher F. Comparison of Y-doped $BaZrO_3$ thin films for high temperature humidity sensors by RF sputtering and pulsed laser deposition. Sen Actuators B: Chem. 2010; 148(1):173-180. https://doi.org/10.1016/j.snb.2010.03.074
17. Gao DY, Guo RS. Densification and properties of barium zirconate ceramics by addition of P_2O_5. Mater Lett. 2010; 64(5):573-575. https://doi.org/10.1016/j.matlet.2009.12.003
18. Giannici F, Longo A, Kreuer KD, Balerna A, Martorana A. Dopants and defects: Local structure and dynamics in barium cerates and zirconates. Solid State Ion. 2010; 181(3-4):122-125. https://doi.org/10.1016/j.ssi.2009.01.021
19. Laulhe C, Pasturel A, Hippert F, Kreisel J. Random local strain effects in homovalent-substituted relaxor ferroelectrics: A first-principles study of $BaTi_{0.74}Zr_{0.26}O_3$. Phys Rev B. 2010; 82(13):132102. https://doi.org/10.1103/physrevb.82.132102
20. Giannici F, Longo A, Balerna A, Kreuer KD, Martorana A. Proton dynamics in In: $BaZrO_3$: Insights on the atomic and electronic structure from X-ray absorption spectroscopy. Chem mater. 2009; 21(13):2641-2649. https://doi.org/10.1021/cm803379n
21. Park JS, Lee JH, Lee HW, Kim BK. Low temperature sintering of $BaZrO_3$-based proton conductors for intermediate temperature solid oxide fuel cells. Solid State Ion. 2010; 181(3-4):163-167. https://doi.org/10.1016/j.ssi.2009.06.015
22. Peng C, Melnik J, Luo JL, Sanger AR, Chuang KT. $BaZr_{0.8}Y_{0.2}O_{3-\delta}$ electrolyte with and without ZnO sintering aid: Preparation and characterization. Solid State Ion. 2010; 181(29-30):1372-1377. https://doi.org/10.1016/j.ssi.2010.07.026
23. Pandurangappa C, Pratibha S. Impact of alkali metal cation (Li^+) on luminescence behavior of $CaSO_4$: Ce^{3+} nanophosphors. Inorg Chem Commun. 2021; 125:108466. https://doi.org/10.1016/j.inoche.2021.108466
24. Abriel W. Calcium sulfatsubhydrat, $CaSO_{4.0}$, $8H_2O$. Acta Crystallogr Sect C Cryst Struct Commun. 1983; 39(8):956-958.

25. Cullity BD, Smoluchowski R. Elements of X-ray diffraction. Phys Today. 1957; 10(3):50.
26. Williamson GK, Hall WH. X-ray line broadening from filed aluminium and wolfram. Acta metall. 1953; 1(1):22-31.
27. Katyayan S, Agrawal S. Study of optical behaviour of Eu^{3+} and Tb^{3+} doped zirconate perovskite phosphors prepared by molten salt technique. Opt Quantum Electron. 2020; 52(18). https://doi.org/10.1007/s11082-019-2129-9
28. Miranda EAC, Carvajal JFM, Baena OJR. Effect of the fuels glycine, urea and citric acid on synthesis of the ceramic pigment $ZnCr_2O_4$ by solution combustion. Mater Res. 2015; 18(5):1038-1043. https://doi.org/10.1590/1516-1439.019915
29. Abimalar J, Ferby VA. Structural, electrical, optical and phase investigation of perovskite barium zirconate ($BaZrO_3$) nanoparticles prepared through auto-combustion technique. Nanosyst Phys Chem Math. 2023; 14(4):467-478. https://doi.org/10.17586/2220-8054-2023-14-4-467-478
30. Romero VH, Rosa ED, Salas P, Salazar JJV. Strong blue and white photoluminescence emission of $BaZrO_3$ undoped and lanthanide doped phosphor for light emitting diodes application. J Solid State Chem. 2012; 196:243-248. https://doi.org/10.1016/j.jssc.2012.06.026
31. Dhahri KK, Bejar M, Dhahri E, Graca MFP, *et al*. Blue-green photoluminescence in $BaZrO_{3-\delta}$ powders. Chem Phys Lett. 2014; 610-611:341-344. https://doi.org/10.1016/j.cplett.2014.07.057
32. Azizi M, Paydar MH, Alafzadeh M. Influence of the calcination temperature and fuel composition on synthesis of Bazr0.8y0.203-δ by solution combustion method for high proton conductivity. Int J Adv Sci Technol. 2016; 96:11-20. https://doi.org/10.14257/ijast.2016.96.02
33. Siddaramanna A, Rao BM, Khosla A, *et al*. Investigations on the effect of NH_4Cl flux on the structural and optical properties of $CdSiO_3$:Eu^{3+} nanophosphor. Mater Res Innov. 2022; 26(7):437-445. https://doi.org/10.1080/14328917.2022.2044172
34. Hunt RW, Pointer MR. Measuring colour. John Wiley and Sons; 2011.
35. Shivakumar J, Krishna RH, Ashoka S, Nagaraju G. $CdSiO_3$:Eu^{3+} nanophosphor: One pot synthesis and enhancement of Orange-red emission through Li^+ co-doping. J Mater Sci Mater Electron. 2018; 29:12986-12992. https://doi.org/10.1007/s10854-018-9419-z
36. Madhukumar K, Babu KR, Prasad KCA, James J, Elias TS, Padmanabhan V, Nair CMK. Thermoluminescence dosimetry of rare earth doped calcium aluminate phosphors. Bull Mater Sci. 2006; 29:119-122. https://doi.org/10.1007/bf02704603
37. Sharma G, Chawla P, Lochab SP, Singh N. Thermoluminescence characteristics of CaS: Ce nanophosphors. CHL. 2009; 6(12):705-712.
38. Gartia RK, Singh SD, Mazumdar PS. Computerized glow curve deconvolution: The case of LiF TLD-100. J Phys D: Appl Phys. 1993; 26(5):858. https://doi.org/10.1088/0022-3727/26/5/021
39. Vij A, Lochab SP, Singh N, Kumar R, Singh N. Thermoluminescence response and trap parameters determination of gamma exposed Ce doped SrS nanostructures. J Alloys Compd. 2010; 490(1-2):L33-L36. https://doi.org/10.1016/j.jallcom.2009.10.075
40. Meijerink A, Blasse G, Glasbeek M. Photoluminescence, thermoluminescence and EPR studies on $Zn_4B_6O_{13}$. J Phys Condens Matter. 1990; 2(29):6303. https://doi.org/10.1088/0953-8984/2/29/008
41. Yukihara EG, Gaza R, McKeever SWS, Soares CG. Optically stimulated luminescence and thermoluminescence efficiencies for high-energy heavy charged particle irradiation in Al_2O_3:C. Radiat Meas. 2004; 38(1):59-70. https://doi.org/10.1016/s1350-4487(03)00251-8
42. Yang B, Fan Y, Lu Q, Townsend PD. Effects of the thermal annealing on the traps and recombination centres in LiF: Mg, Cu, P thermoluminescence dosimeter. Nucl Instrum Methods Phys Res B. 2003; 211(4):577-583. https://doi.org/10.1016/s0168-583x(03)01517-9
43. Tang K. Dependence of thermoluminescence in LiF: Mg, Cu, Na, Si phosphor on Na dopant concentration and thermal treatment. Radiat Meas. 2003; 37(2):133-140. https://doi.org/10.1016/s1350-4487(02)00171-3
44. Drozdowski W, Wisniewski D, Wojtowicz AJ, Lempicki A, Dorenbos P, Haas JTM, Eijk CWEV, Bos AJJ. Thermoluminescence of $LuAlO_3$: Ce. J Lumin. 1997; 72-74:756-758. https://doi.org/10.1016/s0022-2313(96)00212-8
45. Bos AJJ. On the energy conversion in thermoluminescence dosimetry materials. Radiat meas. 2001; 33(5):737-744. https://doi.org/10.1016/s1350-4487(01)00094-4
46. Lin Y, Tang Z, Zhang Z, Nan C. Influence of co-doping different rare earth ions on the luminescence of $CaAl_2O_4$-based phosphors. J Eur Ceram Soc. 2003; 23(1):175-178. https://doi.org/10.1016/s0955-2219(02)00080-8
47. Yukihara EG, Whitley VH, Polf JC, Klein DM, McKeever SWS, Akselrod AE, Akselrod MS. The effects

of deep trap population on the thermoluminescence of Al_2O_3: C. Radiat meas. 2003; 37(6):627-638. https://doi.org/10.1016/s1350-4487(03)00077-5

48. Justel T, Lade H, Mayr W, Meijerink A, Wiechert DU. Thermoluminescence spectroscopy of Eu^{2+} and Mn^{2+} doped $BaMgAl_{10}O_{17}$. J Lumin. 2003; 101(3):195-210. https://doi.org/10.1016/s0022-2313(02)00413-1
49. Schipper WJ, Blasse G, Leblans P. Nb (V) as an electron trap in the storage phosphor $Ba_5SiO_4Br_6$: Eu (II), Nb (V). Chem mater. 1994; 6(10):1784-1789. https://doi.org/10.1021/cm00046a035
50. Furetta C. Handbook of thermoluminescence. World Scientific. 2010.
51. Chen R, Kirsh Y. Analysis of thermally stimulated processes. Pergamon Press. 1981.
52. Halperin A, Braner AA. Evaluation of thermal activation energies from glow curves. Phys Rev. 1960; 117(2):408. https://doi.org/10.1103/physrev.117.408
53. Lushchik C. The investigation of trapping centers in crystals by the method of thermal bleaching. J Exp Theor Phys. 1956; 3(3):390-399.
54. Chen R. Glow curves with general order kinetics. J Electrochem Soc. 1969; 116(9):1254. https://doi.org/10.1149/1.2412291
55. Silpa TN, Pandurangappa C, Yashaswini, Pratibha S. Cost--effective synthesis of Eu^{3+}-activated $BaZrO_3$ for optoelectronic and dosimetry applications. Journal of Electronic Materials. 2025: 1-16.
56. Halperin A, Braner AA. Evaluation of thermal activation energies from glow curves. Phys Rev. 1960; 117(2):408. https://doi.org/10.1103/physrev.117.408
57. Chen R. On the calculation of activation energies and frequency factors from glow curves. J Appl Phys. 1969; 40(2):570-585. https://doi.org/10.1063/1.1657437
58. Lingappa A, Manohara BM. Effect of Gd^{3+} substituted Cadmium silicate nanophosphor for dosimetric applications. J Lumin. 2022; 241:118476. https://doi.org/10.1016/j.jlumin.2021.118476
59. Jahan MS, Cooke DW, Hults WL, Smith JL, Bennett BL, Maez MA. Thermally stimulated luminescence from commonly occuring impurity phases in high-temperature superconductors. J Lumin. 1990; 47(3):85-91. https://doi.org/10.1016/0022-2313(90)90003-t
60. Furretta C. Hand book of thermoluminescences. World Scientific Publishing Co. Pvt. Ltd. 2003.
61. Flores NV, Juarez CJS, Esquivel RIL, Altamirano DN, Valdes MAU, Olguin JCG, *et al*. Thermally stimulated luminescence of $BaZrO_3$: Eu^{3+} nanopowders for dosimetric applications. Opt Mater. 2024; 147:114740. https://doi.org/10.1016/j.optmat.2023.114740
62. Mendoza MM, Melendrez R, Gonzalez LA. Thermoluminescence of beta irradiated $SrHfO_3$ powders synthesized by the Pechini-type sol-gel method. J Lumin. 2023; 263:120048. https://doi.org/10.1016/j.jlumin.2023.120048